Driving towards cost-competitive biofuels through catalytic fast pyrolysis by rethinking catalyst selection and reactor configuration

Journal:	*Energy & Environmental Science*
Manuscript ID	EE-ART-06-2018-001872.R1
Article Type:	Paper
Date Submitted by the Author:	01-Aug-2018

Complete List of Authors:	Griffin, Michael; National Renewable Energy Laboratory, National Bioenergy Center Iisa, Kristiina; National Renewable Energy Laboratory, National Bioenergy Center Wang, Huamin; Pacific Northwest National Laboratory , Dutta, Abhijit; National Renewable Energy Laboratory, National Bioenergy Center Orton, Kellene; National Renewable Energy Laboratory, French, Richard; National Renewable Energy Laboratory, Santosa, Daniel; Pacific Northwest National Laboratory, Wilson, Andrew; National Renewable Energy Laboratory, National Bioscience Center Christensen, Earl; National Renewable Energy Laboratory, Center for Transportation Technologies and Systems Nash, Connor; National Renewable Energy Laboratory, National Bioenergy Center Van Allsburg, Kurt; National Renewable Energy Laboratory, National Bioenergy Center Baddour, Frederick; National Renewable Energy Laboratory, National Bioenergy Center Ruddy, Daniel; National Renewable Energy Laboratory, Chemical and Materials Science Center Tan, Eric C. D.; National Renewable Energy Laboratory, National Bioenergy Center Cai, Hao; Argonne National Laboratory, Systems Assessment Group Mukarakate, Calvin; National Renewable Energy Laboratory, National Bioenergy center Schaidle, Joshua; National Renewable Energy Laboratory, National Bioenergy Center

Energy & Environmental Science

PAPER

Driving towards cost-competitive biofuels through catalytic fast pyrolysis by rethinking catalyst selection and reactor configuration

Michael B. Griffin,[a,‡] Kristiina Iisa,[a,‡] Huamin Wang,[b] Abhijit Dutta,[a] Kellene A. Orton,[a] Richard J. French,[a] Daniel M. Santosa,[b] Nolan Wilson,[a] Earl Christensen,[a] Connor Nash,[a] Kurt M. Van Allsburg,[a] Frederick G. Baddour,[a] Daniel A. Ruddy,[a] Eric C. D. Tan,[a] Hao Cai,[c] Calvin Mukarakate,[a] Joshua A. Schaidle[a,*]

Received 00th January 20xx,
Accepted 00th January 20xx

DOI: 10.1039/x0xx00000x
www.rsc.org/ees

Catalytic fast pyrolysis (CFP) has emerged as an attractive process for the conversion of lignocellulosic biomass into renewable fuels and products. Considerable research and development has focused on using circulating-bed reactors with zeolite catalysts (e.g., HZSM-5) for CFP because of their propensity to form gasoline-range aromatic hydrocarbons. However, the high selectivity to aromatics comes at the expense of low carbon yield, a key economic driver for this process. In this contribution, we evaluate non-zeolite catalysts in a fixed-bed reactor configuration for an integrated CFP process to produce fuel blendstocks from lignocellulosic biomass. These experimental efforts are coupled with technoeconomic analysis (TEA) to benchmark the process and guide research and development activities to minimize costs. The results indicate that CFP bio-oil can be produced from pine with improved yield by using a bifunctional metal-acid 2 wt% Pt/TiO_2 catalyst in a fixed-bed reactor operated with co-fed H_2 at near atmospheric pressure, as compared to H-ZSM5 in a circulating-bed reactor. The Pt/TiO_2 catalyst exhibited good stability over 13 reaction-regeneration cycles with no evidence of irreversible deactivation. The CFP bio-oil was continuously hydrotreated for 140 h time-on-stream using a single-stage system with 84 wt% of the hydrotreated product having a boiling point in the gasoline and distillate range. This integrated biomass-to-blendstock process was determined to exhibit an energy efficiency of 50% and a carbon efficiency of 38%, based on the experimental results and process modelling. TEA of the integrated process revealed a modelled minimum fuel selling price (MFSP) of $4.34 per gasoline gallon equivalent (GGE), which represents a cost reduction of $0.85 GGE^{-1} compared to values reported for CFP with a zeolite catalyst. TEA also indicated that catalyst cost was a significant factor influencing the MFSP, which informed additional CFP experiments in which lower-cost Mo_2C and high-dispersion 0.5 wt% Pt/TiO_2 catalysts were synthesized and evaluated. These materials demonstrated CFP carbon yield and oil oxygen content similar to that of the 2 wt% Pt/TiO_2 catalyst, offering proof-of-concept that the lower-cost catalysts can be effective for CFP and providing a route to reduce the modelled MFSP to $3.86-3.91 GGE^{-1}. This report links foundational science and applied engineering to demonstrate the potential of fixed-bed CFP and highlights the impact of coupled TEA to guide research activities towards cost reductions.

Broader context

According to a 2016 report from the U.S. Department of Energy, an annual supply of over one billion tons of biomass can be made available for energy applications in the United States without adversely affecting the environment or impacting food supplies. In order to utilize this abundant resource, new technologies must be developed which are compatible with lignocellulosic feedstocks. To this end, catalytic fast pyrolysis (CFP) offers a promising route to convert many different types of lignocellulose into bio-fuels and bio-products. However, improvements in carbon yield are necessary to improve the economics of the process. In this contribution, we build on existing computational, model compound, and microscale research to offer a first-of-its-kind technical and economic evaluation of fixed-bed hydrodeoxygenation catalysts as part of an integrated biomass-to-blendstocks process. The results underscore the potential of fixed-bed CFP and highlight the value of using technoeconomic analysis as a guide for research and development activities.

1. Introduction

In a 2016 report from the United States Department of Energy, it was estimated that more than one billion tons of biomass can be made available for energy applications while still meeting food, feed, forage, and fiber demands and with minimal or negligible environmental effects. This amount of biomass could be used to offset approximately 31% of 2017 U.S. petroleum consumption through the production of biofuels, biopower, and bioproducts.[1, 2] Utilizing this abundant resource will require the development of a robust bioeconomy with new technologies to efficiently convert lignocellulosic biomass into liquid transportation fuels, which have the potential to provide a critical energy source that is compatible

[a] *National Renewable Energy Laboratory, 15523 Denver West Pkwy., Golden, CO 80401, USA.*
[b] *Pacific Northwest National Laboratory, 902 Battelle Blvd., Richland, WA 99352 USA*
[c] *Argonne National Laboratory, 9700 Cass Ave., Lemont, IL 60439*
‡ These authors contributed equally to the article.
* Corresponding author: Joshua.Schaidle@nrel.gov
† Electronic Supplementary Information (ESI) available: See
DOI: 10.1039/x0xx00000x

with current infrastructure and can be realized on a relatively short time scale.[3, 4] Identifying routes to sustainable fuels is particularly important for the heavy vehicle transportation sector, where electric and hybrid technologies are less developed. To this end, fast pyrolysis offers a promising technology for the conversion of lignocellulosic biomass into renewable bio-oil.[4-7] Bio-oil can be used to supplement traditional fossil-derived oil through the development of refinery co-processing approaches, but there are major chemical differences between these materials that must be addressed before bio-oil is suitable for use as a direct drop-in transportation fuel or blendstock.[8, 9] Of primary concern is the high concentration of chemically-bound oxygen in bio-oil (up to 40 wt%), which contributes to a number of undesirable characteristics including low heating value, high acidity, and chemical instability.[10] Consequently, the deoxygenation of bio-oil is a critical step to enable the production of transportation fuels from biomass pyrolysis at the industrial scale.

Ex situ catalytic fast pyrolysis (CFP) is a technique in which biomass pyrolysis vapors are sent to a secondary reactor where they are catalytically deoxygenated prior to condensation. The CFP-derived bio-oil, or "CFP-oil", exhibits improved properties (e.g., stability, heating value, hydrocarbon miscibility) and may either be utilized directly, hydrotreated to finished fuels in a stand-alone unit, or further processed in existing refinery infrastructure.[4] The CFP process is conducted at near atmospheric pressure, differentiating it from hydropyrolysis approaches where hydrogen pressures of 1.4-20 MPa are utilized during the pyrolysis and catalytic upgrading steps.[11-14] The comparatively low pressure requirement for CFP has the potential to reduce capital costs and mitigate technical issues associated with the introduction of low density biomass into pressurized systems. Zeolites such as HZSM-5 are commonly employed in CFP processes because they produce gasoline-range aromatic hydrocarbons.[15-20] However, these reactions also form light gasses such as CO, CO_2, and olefins, which reduce the carbon efficiency of the process. Additional carbon losses over HZSM-5 occur due to catalyst coking, which leads to rapid deactivation and necessitates the use of circulating-bed reactor systems to facilitate frequent regeneration cycles. For example, pilot-scale experiments performed at a biomass feed rate of 20 kg/h produced bio-oil with 24% carbon yield and 22 wt% oxygen content.[17] Other experimental studies have reported values corresponding to carbon yields of 21-33% for oils with 18-24 wt% oxygen.[21-24] Consequently, the yield of gasoline-range products during CFP with HZSM-5 remains on the order of 50% of the theoretical maximum.[25] Based on technoeconomic analysis (TEA), carbon yield to fuel products has been identified as a key economic driver in determining the minimum fuel selling price (MFSP). A benchmark value of 33% for CFP-oil carbon yield (with 17 wt% oxygen) has been reported to correspond a MFSP of \$5.19 GGE^{-1} (gallons of gasoline equivalent) for a CFP process using HZSM-5 in a circulating-bed reactor followed by hydrotreating to produce liquid fuels.[24, 26] Ongoing research is continuing to reduce the costs of this pathway through process and catalyst optimization, but alternative CFP approaches with non-zeolite catalysts hold the potential to increase carbon yield and thereby boost cost competitiveness with current lower cost fossil-based pathways.

The use of bifunctional metal-acid catalysts to promote hydrodeoxygenation (HDO) offers an alternative CFP approach which has been previously outlined in a conceptual design and is illustrated in Fig. 1.[27] This process, in which hydrogen is utilized to remove oxygen as water, has the potential to improve carbon yields by minimizing the production of carbon-containing light gasses and reducing catalyst coking.[28] Lower rates of coking compared to HZSM-5 also increase catalyst stability and enable the use of fixed-bed reactors, which exhibit minimal attrition compared to circulating- or fluidized-bed reactors. The corresponding improvements in catalyst lifetime create the opportunity to explore higher-cost, bifunctional catalysts which provide access to a broader range of chemistries and improved control over product composition.

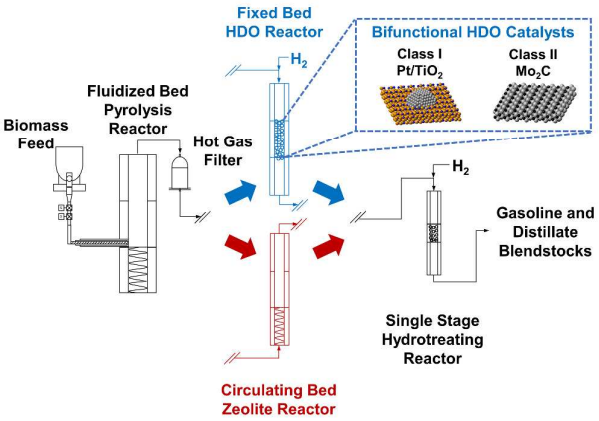

Fig. 1 Simplified diagram outlining an integrated CFP process for the production of hydrocarbon blendstocks via fixed-bed HDO (blue) or circulating-bed zeolite upgrading (red) of biomass pyrolysis vapors.

Metal-acid bifunctionality has been identified as a critical design criterion for the development of HDO catalysts, and catalyst development has focused primarily on two classes of bifunctional materials. To simplify discussion in this manuscript, we have defined these two classes as follows: (Class I) a metallic phase dispersed on an acidic support and (Class II) a single active phase possessing a combination of metal and acid sites. For example, Class I catalysts comprised of noble metals (e.g., Pt, Pd, Ru) dispersed on reducible/amphoteric oxide supports (e.g., TiO_2, ZrO_2) have demonstrated activity for the direct deoxygenation of lignin-derived aromatic oxygenates (e.g., phenol, m-cresol, guaiacol, anisole).[29-36] The high performance of these catalysts has been attributed to cooperative effects between metallic and acidic sites at or near the active phase-support interface.[29-31, 33, 36] Likewise, it has been proposed that the co-location of metallic and acidic sites promotes HDO over Class II catalysts such as molybdenum carbide (Mo_2C), which has been identified as an effective catalyst for the deoxygenation of lignin-derived[37-40]

and carbohydrate-derived model compounds.[41, 42] Although full understanding of the underlying surface chemistry has yet to be achieved, it has been proposed that tuning the ratio of acidic to metallic sites may allow for tailored reactivity, and values in the range 4.6–26 have been reported to correspond with desirable deoxygenation performance.[31, 40-44] Molybdenum oxide (MoO_3) has also been demonstrated to be an effective Class II catalyst for the deoxygenation of pyrolysis vapor model compounds.[45-47] It has been reported that MoO_3 undergoes partial carburization during reaction to from oxycarbide- and oxycarbohydride-containing phases, indicating that surface carbon may play an important role in the activity of MoO_3 under HDO conditions.[46]

Although model compound experiments have provided valuable insight into deoxygenation pathways and mechanisms, less is known about the effectiveness of bifunctional HDO catalysts for the upgrading of whole biomass pyrolysis vapors. Lu and co-workers utilized a qualitative microscale fixed-bed reactor system operated at 600 °C in the absence of hydrogen to evaluate a series of Class I catalysts for the deoxygenation of poplar wood pyrolysis vapors.[48] The authors determined that catalysts comprised of Ru or Pd supported on CeO_2-impregnated TiO_2 or ZrO_2-TiO_2 effectively reduced the yields of undesired phenols, acids, and sugars compared to a non-catalytic process. In a separate report, Wan and co-workers[49] evaluated Ru/TiO_2 as a fixed-bed catalyst for the upgrading of oak and switchgrass pyrolysis vapors at 400 °C and 0.058 MPa H_2. The authors reported that Ru/TiO_2 converted light oxygenates to larger, less oxygenated molecules and improved the stability of the upgraded bio-oil. Among Class II catalysts, it has been reported that Mo–C/Al_2O_3 is effective for upgrading pine pyrolysis vapors to produce aliphatic and aromatic hydrocarbons in a microscale fixed-bed pulsed reactor, albeit at low biomass:catalyst (B:C) ratios.[50] A microscale fixed-bed pulsed reactor was also utilized to evaluate MoO_3/TiO_2 and MoO_3/ZrO_2 for the deoxygenation of pine pyrolysis vapors.[51] The supported-MoO_3 catalysts exhibited complete deoxygenation to olefinic and aromatic hydrocarbons at B:C ratios < 1.5, some production of partially deoxygenation species at B:C ratios from 1.5-5, and breakthrough of primary pyrolysis vapors at B:C ratios > 5. The deoxygenation performance of molybdenum-based reducible metal oxide catalysts has also been evaluated using a lab-scale fluidized bed reactor and was reported to convert pine pyrolysis vapors into a hydrocarbon-rich products with a carbon yield and oxygen content of 43.2% and 6.2 wt%, respectively.[52] Collectively, these data highlight the promising HDO performance of bifunctional metal-acid catalysts. However, catalyst attrition during fluidized-bed experiments has yet to be evaluated, and long-term catalyst stability in dynamic beds remains uncertain. For reports on fixed-bed upgrading, all experiments were performed at a ≤6 g_{cat} scale, often using pulsed reactor systems which do not necessarily probe catalyst stability or reflect continuous upgrading conditions. In all cases, the impact of catalyst performance on the economics of the overall process remain uncertain, and limited research has been performed to understand the impact of CFP on downstream hydrotreating steps or to evaluate the fuel properties of the resulting product. Consequently, there is lack of understanding regarding how results from fundamental microscale/model compound experiments can be translated to applied process development, which leads to many open questions regarding the feasibility of fixed-bed CFP at the commercial scale.

In this contribution we help bridge this research gap by evaluating the performance of bifunctional 2 wt% Pt/TiO_2 for the continuous upgrading of pine pyrolysis vapors using a large bench-scale reactor and 100 g of catalyst. Stability was assessed during 13 regeneration cycles, and the upgraded bio-oil product was condensed, hydrotreated, and fractionated into the gasoline and diesel range, which were subsequently analysed to determine their fuel properties. These data were used to develop process models and perform technoeconomic analysis (TEA) of the integrated *ex situ* CFP process using 2 wt% Pt/TiO_2. TEA results informed additional CFP experiments, which were performed with lower-cost bifunctional 0.5 wt% Pt/TiO_2 and Mo_2C to demonstrate routes towards additional reductions in MFSP. The results highlight the potential for high carbon yields during fixed-bed CFP and identify economically impactful technical targets to guide future research.

2. Results and discussion

2.1 Catalyst Characterization

A 2 wt% Pt/TiO_2 catalyst was prepared using standard incipient wetness impregnation methods described in Sec. 4.2. The average Pt particle diameter, Pt loading, Pt dispersion, metal site density, and acid site density are given in Table 1. Representative TEM images of the 2 wt% Pt catalysts, as well as the Pt particle size distribution, are shown in Fig. S1a-b. The TEM images indicate spherical and quasi-spherical Pt particles with an average diameter of 2.7 ± 1.2 nm, but particles as large as 26 nm were observed. The BET surface area of the catalyst was determined to be 44 $m^2\ g^{-1}$. The measured Pt loading was 2.4 wt%, which is lower than the targeted 5 wt% loading. The lower than expected Pt loading may be due to incomplete impregnation of the TiO_2 extrudates and/or loss of crystallized Pt precursor from the external surface of the extrudate during material transfer and handling. The measured value was confirmed with repeat analyses and was used for all calculations reported in this manuscript. The Pt dispersion was determined to be 33% by CO chemisorption, which is suggestive of particles with an average diameter of 3.6 nm and is generally consistent with the average particle diameter measured by TEM (2.7 ± 1.2 nm). The temperature programmed desorption (TPD) profile used to determine acid site density (220 μmol g^{-1}) consists of a single NH_3 desorption peak centered near 350 °C (Fig. S2a). This temperature is lower than the 375 °C value which has been previously reported for HZSM-5, suggesting that the Pt/TiO_2 catalyst contain sites with slightly weaker acid strength.[53] It has also been reported that TiO_2 is primarily Lewis acidic due to coordinatively unsaturated Ti centers, which is in contrast to primarily Brønsted acidic zeolite catalysts.[44] The X-ray diffraction (XRD) pattern for the

reduced Pt/TiO_2 catalyst confirms the presence of metallic Pt and crystalline TiO_2 (Fig. S3a). The support was comprised of 90% anatase and 10% rutile TiO_2, as determined by Rietveld analysis. Based on these characterization data, this Pt/TiO_2 material is a representative Class I bifunctional catalyst with an acid:metal site ratio of 5.5, which is in the range of 4.6-26 reported for other bifunctional catalysts which have demonstrated activity for deoxygenation of biomass-derived model compounds.[31, 40, 42, 44]

Table 1. The Pt diameter (TEM), Pt loading (ICP), Pt dispersion (CO chemisorption), metal site density (CO chemisorption), and acid site density (NH_3-TPD) measured over the reduced Pt/TiO_2 catalyst prior to reaction testing. Error bars represent ± σ.

Pt diameter (nm)	Pt loading (wt%)	Pt dispersion (%)	Metal site density (μmol g^{-1})	Acid site density (μmol g^{-1})	Acid: metal site ratio
2.7 ± 2.4	2.4	33	40	220	5.5

2.2 CFP Reaction Testing and Post-Reaction Catalyst Characterization

Thirteen sequential CFP reaction/regeneration cycles were performed in a fixed-bed flow reactor operated at 400 °C and 0.08 MPa H_2. During each reaction, a continuous feed of pine was introduced at a weight hourly space velocity (WHSV) of 1.5 h^{-1}, which is defined in terms of the gravimetric feed rate of biomass to the pyrolysis reactor and the total catalyst mass in the fixed-bed reactor. Once a cumulative B:C ratio of 2.8-3.0 was achieved, the flow of pine was stopped, and the catalyst was regenerated via thermal oxidation and reduction to begin the next cycle. Real time monitoring of the vapor effluent indicates that the product distribution changed significantly during each 2 h reaction cycle. These changes would not be captured by reaction testing performed using a microscale pulsed system at low B:C ratio and reflect the importance of assessing the dynamic nature of catalyst performance in continuous reaction environments. Mass spectrometer traces representative of major compound classes are shown in Fig. 2a. The concentration of toluene, which reflects the trends exhibited by aromatic hydrocarbons, decreased sharply during the first 15 minutes, followed by a more gradual decline over the rest of the reaction period. The concentration of acetone, furan, and phenol, which reflect the trends exhibited by partially upgraded oxygenates, exhibited a corresponding increase during the early stages of the reaction before stabilizing and ultimately decreasing slightly. The concentration of acetic acid and methoxyphenol, which reflect the trends exhibited by unreacted oxygenates, did not undergo rapid changes during the initial 15 min. Instead, the concentration of these compounds increased steadily over the entire reaction period. These shifts in selectivity suggest that the catalyst quickly undergoes an initial deactivation period followed by a more gradual decline in activity. Similar trends were observed during experiments performed over the TiO_2 support in the presence of hydrogen (Fig. 2b), but in this case there was a decreased production of aromatic hydrocarbons and a more rapid breakthrough of unreacted oxygenates. In contrast, minimal production of aromatic hydrocarbons was detected during experiments performed over TiO_2 under inert conditions (Fig. 2c), and partially upgraded or unreacted oxygenates were the dominant class of products during the entire reaction period. Collectively, these data suggest that the presence of Pt enhanced the activity and/or prolonged the lifetime of TiO_2 active sites under reducing conditions. Similar results have been reported in model compound experiments, where hydrogen spillover from the metal is proposed to form Lewis-acidic oxygen vacancies on TiO_2 which are capable of aryl-OH bond scission.[31, 44] Hydrogen spillover from Pt may also prolong lifetime by facilitating the removal of coke precursors from the catalyst surface (*vide infra*). The initial deactivation period over Pt/TiO_2 also corresponded with a decrease in the C_2-C_3 alkane concentration and an increase in the C_2-C_3 alkene concentration (Fig. S4). These data reveal a loss of hydrogenation activity, which may be associated with the blocking of metallic Pt sites.

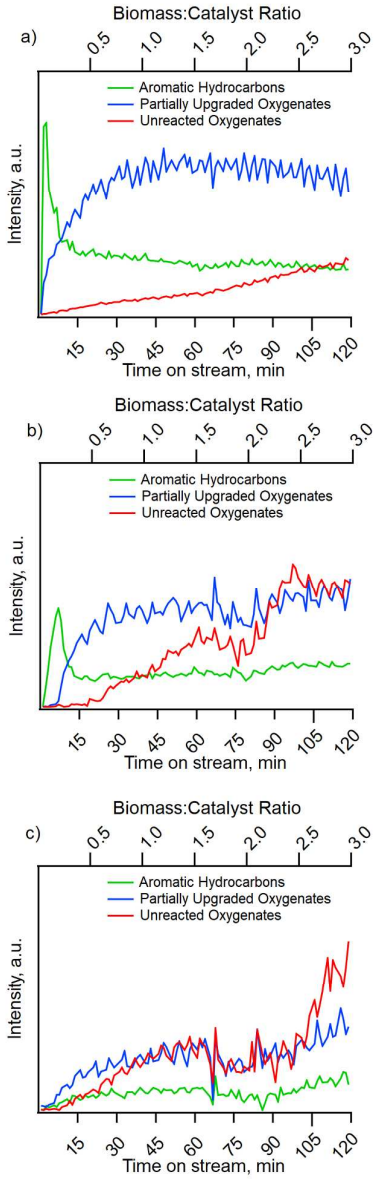

Fig. 2 Intensities of selected m/z signals observed over (a) 2 wt% Pt/TiO_2 in 85% H_2/N_2, (b) TiO_2 in 85% H_2/N_2, and (c) TiO_2 in N_2. The trace labeled "aromatic hydrocarbons" represents m/z=91, which is derived from toluene. The trace labeled "partially upgraded oxygenates" represent the sum of m/z=58, 68, and 94, which are derived from acetone, furan, and phenol, respectively. The trace labeled "unreacted oxygenates" represents the sum of m/z=60 and 124, which are derived from acetic acid/hydroxyacetaldehyde and methoxyphenol, respectively.

To gain further insight into catalyst stability, a regenerated sample of post-reaction Pt/TiO_2 was characterized by TEM (Fig. S1c-d), NH_3-TPD (Fig. S2b), XRD (Fig. S3b), and N_2 physisorption. The average Pt particle size measured by TEM increased from 2.7 ± 1.2 nm on the pre-reaction sample to 4.4 ± 1.6 nm on the post-reaction sample. This increase in Pt particle size is consistent with the CO uptake observed during chemisorption experiments, which decreased from 40 to 15 μmol g^{-1} for the pre- and post-reaction samples, respectively. The growth of Pt particles is likely due to thermal sintering during the reaction or during regeneration, when coke oxidation can lead to highly localized temperature spikes. Post-reaction NH_3-TPD indicates an acid site density of 210 μmol g^{-1}, which is similar to the value of 220 μmol g^{-1} for the pre-reaction catalyst. Likewise, no change in the maximum NH_3 desorption temperature was observed, suggesting that there was no change to the strength of the acid sites between pre-reaction and post-reaction samples. Based on data from CO chemisorption and NH_3-TPD, the acid:metal site ratio was determined to increase from 5.5 to 14 for the pre- and post-reaction samples, respectively. However, both of these values are within the range of ratios reported for other bifunctional catalysts which are active for deoxygenation of biomass-derived model compounds.[31, 40, 42, 44] The post-reaction XRD indicates that TiO_2 remains mixed phase, with a slight reduction in anatase content (85% vs 90%) and increase in the rutile content (15% vs 10%) compared to the pre-reaction catalyst. The surface area of the post-reaction, regenerated catalyst was 46 m^2 g^{-1}, which is similar to the pre-reaction measurement of 44 m^2 g^{-1}. These analyses demonstrate that there were minimal changes to the TiO_2 support. The measured increase in Pt particle size did not have an apparent impact on performance, which remained relatively constant over a thirteen-cycle experimental period (Fig. 3).

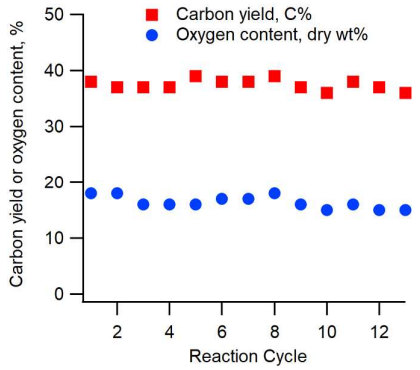

Fig. 3 The CFP-oil carbon yield and oxygen content on dry basis for each reaction cycle over 2 wt% Pt/TiO_2.

The total production of CFP bio-oil during the 13 reaction cycles was 750 mL. The CFP-oil compositions and yields for each experimental cycle are provided in Table S1, and the averaged values are reported in Table 2. The average CFP-oil carbon yield obtained from Pt/TiO_2 was 38%, which represents a significant improvement compared to values of 21-33% reported for HZSM-5-derived CFP-oils with similar oxygen concentration.[17, 21-24] The comparatively high carbon yield for Pt/TiO_2 is primarily attributed to a reduction in catalyst coking, which accounted for only 6% of the biomass carbon in these experiments. In contrast, approximately 12% of biomass

carbon is converted to coke over HZSM-5 when producing oils with similar oxygen contents.[22] Coke formation in zeolite micropores is a well-known consequence of hydrocarbon-pool chemistry.[54] The reduction in coking over Pt/TiO_2 may be due to hydrogenation of strongly bound adsorbates on the TiO_2 surface, which leads to desorption and retention of these species in the bio-oil. This enhancement in hydrogenation activity is consistent with the high H:C molar ratio of the Pt/TiO_2-derived CFP-oil compared to HZSM-5-derived CFP-oils (1.23 ± 0.02 vs. 1.07-1.17, respectively).[17, 21, 22] Carbon loss to light gases over Pt/TiO_2 was also slightly reduced compared to HZSM-5 (26 % vs. 27-29%).[22, 55] High CFP-oil yields have also been reported during experiments performed over Ru/TiO_2, suggesting that the results observed over Pt/TiO_2 may be generally applicable to other Class I bifunctional metal-acid catalysts.[49]

Table 2. Summary of CFP-oil properties generated over 2 wt% Pt/TiO_2 including mass and carbon yields on dry biomass basis, oil composition on dry basis, and gas yields. Error bars represent ± σ as determined from the 13 individual CFP cycles.

Phase	Yield, wt%	Yield, C%	Oil Composition, wt% dry		Gas Yield, wt%	
Oil	27±1	38±1	C	76±1	CH_4	2.3±0.2
Aq.	25±1	2.8±0.2	H	7.7±0.2	CO	14±0.8
Gas	30±1	26±1	N	0.2±0.0	CO_2	8.2±0.6
Char	10±1	14±1	O	16±1	$CO:CO_2$	1.8±0.2
Coke	3.1±0.5	6.3±0.8	H_2O	4.2±0.2	Alkanes	1.8±0.2
Total	94±1	87±2	H:C	1.23±0.02	Alkenes	1.8±0.1

The average oxygen content in the oil was 16 ± 1 wt% on dry basis. Comparatively, the oxygen content of HZSM-5-derived CFP-oils has been reported to range from 18-24 wt% in larger scale reactor systems[17, 21-23] and non-catalytic bio-oils produced under the pyrolysis conditions utilized here have oxygen contents of 34-36 wt% on dry basis.[55, 56] Of the oxygen contained in the feedstock, 10% remained in the oil organic phase, 32% was converted to CO and CO_2, and 49% was converted to H_2O (Table S2).

Compounds in the CFP-oil were identified by semi-quantitative GC-MS, and a summary of the product distribution, categorized by functional groups, is shown in Fig. 4. The individual components and their concentrations can be found in Table S3. The composition of the first cycle was similar to a mixture containing CFP-oil from all cycles (Fig. S5), which provides support that the selectivity of Pt/TiO_2 was not significantly impacted during reaction or regeneration. The CFP-oil consisted of deoxygenated aromatic hydrocarbons, partially upgraded oxygenates, unreacted methoxyphenols, and trace amounts of anhydrosugars. The observation of methoxyphenols and anhydrosugars indicates that some of the pine pyrolysis vapors passed over the catalyst without reacting; however, >80 wt% of the detected compounds were completely or partially deoxygenated. A comparison between the product distribution observed in the Pt/TiO_2-derived CFP oil and reported for ZSM-5-derived CFP-oil reveals several notable differences.[21, 55] Aromatic hydrocarbons, which are formed over zeolite catalysts via the well-established hydrocarbon pool mechanism, have been reported to be the largest product group found in ZSM-5-derived CFP-oil, accounting for 25-50% of the mass spectrometer area for oils with oxygen contents up to 20 wt%.[21, 55] In contrast, aromatic hydrocarbons only accounted for 2-3 wt% of the identified products over Pt/TiO_2. Instead, partially upgraded oxygenates, including simple phenols (i.e., phenols without additional oxygen functional groups) and cycloketones, were the largest identified product groups in the Pt/TiO_2-derived CFP-oil, accounting for 41 wt% and 17 wt% of the identified compounds, respectively. The high concentration of simple phenols and near absence of benzenediols in the Pt/TiO_2-derived CFP-oil is consistent with the deconstruction of larger lignin-derived oxygenates (i.e., pyrolytic lignin) and suggests that demethoxylation of lignin monomers is a major upgrading pathway for this catalyst. The presence of this pathway is also supported by the high concentration of alkylated phenolic species in the Pt/TiO_2-derived CFP-oil (e.g., ethyl-, propyl-, and propenylphenols, Table S3), which are common to monomeric lignin species. Simple phenols have also been reported to constitute up to 10% of the identified compounds in ZSM-5-derived CFP-oil, although these concentrations are smaller than Pt/TiO_2-derived CPF-oils with similar oxygen content.[21, 22, 55] Cyclopentanones and other carbonyl compounds were also detected in higher concentrations over Pt/TiO_2 compared to reported values of 2-4% for ZSM-5.[21, 55] Cyclopentenones in the Pt/TiO_2 CFP-oil could be derived from furanic compounds found in the pyrolysis vapors, which can be converted to cyclopentanones in aqueous solutions at low temperatures (< 200 °C) and high H_2 pressures (4-8 MPa).[57, 58] Previous reports have also indicated that oxide supported-Pt catalysts are capable of converting the lignin-derived model compound guaiacol to cyclopentanone through a combination of ring opening and decarbonylation reactions.[59]

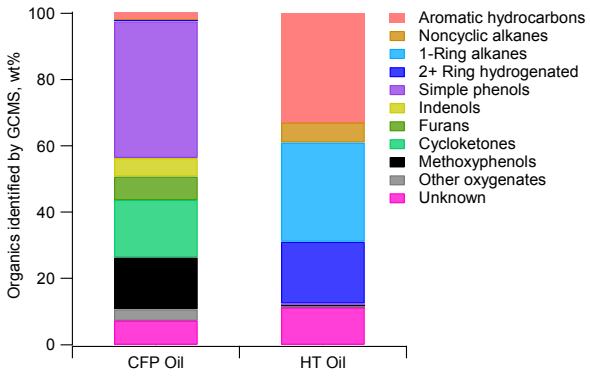

Fig. 4 GC-MS compositional analysis of the 2 wt% Pt/TiO_2-derived CFP-oil and hydrotreated CFP-oil. Identified compounds account for 45 wt% and 46 wt% of the total sample mass for CFP and hydrotreated oil, respectively.

The GC-MS analysis indicated a lower concentration of fully deoxygenated compounds for the Pt/TiO_2-derived CFP-oil than has been reported for ZSM-5-derived CFP-oils with similar oil oxygen content (<3% vs. up to 50%). [21, 55] This apparent discrepancy may be explained by the different species of oxygenates present in each oil. The Pt/TiO_2 catalyst overwhelmingly favors the production of partially upgraded oxygenates with a single oxygen atom. Contrastingly, ZSM-5 catalysts have been reported to produce higher concentrations of oxygenates containing multiple O atoms (e.g., methoxyphenols).[21, 55] Also, it should be emphasized that while GC-MS provides valuable insight into the product distribution, >50 wt% of the oil is not quantified with this method. The remaining material is either present in high-boiling point non-chromatographable compounds, low-boiling point compounds convoluted with elution of the solvent, or compounds that are not adequately separated from other products. The high-boiling point material may contain hemicellulose or lignin oligomers, and the low-boiling material may contain volatile oxygenates and/or hydrocarbons (e.g., acetone, acetic acid, light alkanes). To gain more insight into the full product distribution, the CFP-oils were also analyzed using ^{13}C NMR (Table S4), which allows for quantification of functional groups present in the entirety of the sample. This analysis showed the presence of aromatic C-H, aliphatic C-C, aromatic C-O, C=O, aromatic C-C, aliphatic C-O and C-OCH_3 groups, listed in the order of decreasing abundance. The high aromatic C-H content is derived from a combination of aromatic hydrocarbons and aromatic oxygenates. The greater aliphatic C-C content (31%) compared to values reported for HZSM-5-derived CFP-oils (4-17%)[22, 55] reflects the high H:C ratio of the Pt/TiO_2 CFP-oil, as shown in Table 2. The NMR analysis also confirms the relatively high concentration of carbonyl groups, which is consistent with the GC-MS data in Fig. 4.

2.3 Hydrotreating

The combined CFP-oil was hydrotreated for 82 h in a single stage system operated at 400 °C, 13 MPa total pressure, a H_2/bio-oil ratio of 2700 ml ml^{-1}, and a LHSV of 0.20 h^{-1}. The hydrogen supply was in excess, as is typical for hydrotreating. The yield of major products and the product oil density are plotted in Fig. 5 as a function of time on stream (TOS). The oil density, which provides a measure of fuel quality,[60, 61] increased slightly during hydrotreating, suggesting possible slow deactivation of the Ni-Mo sulfide catalyst. However, no fouling or plugging issues were encountered during this experiment or a subsequent 58 h experiment performed at a higher LHSV using the same catalyst. This stable operation of a single stage hydrotreater for 140 h TOS represents a significant improvement compared to the processing of non-catalytic pyrolysis oil, where rapid plugging leads to process shutdown after approximately 50 h.[61]

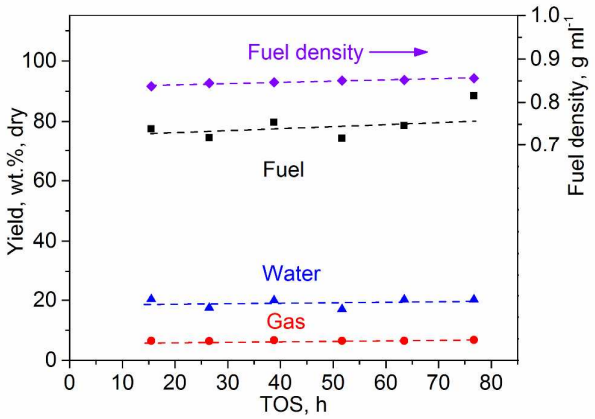

Fig. 5 The mass yield of fuel, water, and gas as a function of TOS during hydrotreating of the CFP-oil mixture with LHSV of 0.2 h^{-1}. Fuel density is included as a measure of the fuel quality.

Analysis of the hydrotreated oil was performed at selected steady-state windows, and the results are summarized in Table 3. The gas and water yields were also determined and are given in Table S5. Hydrotreating reduced the oxygen content of the CFP-oil to approximately 0.4 wt% on dry basis while achieving hydrotreated CFP-oil mass and carbon yields of 76% and 89%, respectively. These yields are consistent with values for other CFP-oils,[55, 62, 63] and are higher than a reported carbon yield of 82% for non-catalytic fast pyrolysis oils.[64] Carbon was lost primarily in the form of CH_4 and C_2-C_5 alkanes, as described in Table S5. CO_2 was also observed, but it represented a minor product and accounted for only 2% of oxygen removal. Most of the oxygen in the CFP-oil was removed as H_2O (ca. 98%). The overall carbon efficiency for the combined process of CFP and hydrotreating was 33%. This result represents a significant improvement over values reported for CFP over HZSM-5 and subsequent hydrotreating (≤22%)[55] due to the higher CFP carbon efficiencies. The hydrogen consumption during hydrotreating of the Pt/TiO_2-derived CFP oil was 0.039 g $g^{-1}_{CFP\text{-}oil}$ (Table S5), which is appreciably lower than reported values for continuous hydrotreating of other CFP-oils (~0.06-0.07 g $g^{-1}_{CFP\text{-}oil}$).[55, 62, 63] This difference is attributed in part to the lower oxygen content of the Pt/TiO_2-derived CFP-oil (16 wt%) compared to values of 19.5 wt%[53] and 22.5 wt%[54] in reported work. Differences in chemical functional groups may also impact hydrogen consumption. For example, cyclopentenones, which were a major product in the Pt/TiO_2-derived CFP-oil, require less hydrogen for deoxygenation and saturation than furans. The relatively high H:C ratio of the Pt/TiO_2-derived CFP-oil (1.23) may also reduce hydrogen demand during the hydrotreating step. However, the combined hydrogen consumption during CFP with Pt/TiO_2 (0.033 g $g^{-1}_{CFP\text{-}oil}$) followed by hydrotreating (0.039 g $g^{-1}_{CFP\text{-}oil}$) was comparable to the hydrogen consumption reported during hydrotreating of oils from CFP performed in the absence of hydrogen (~0.06-0.07 g $g^{-1}_{CFP\text{-}oil}$).[55, 62, 63]

Table 3. Summary of hydrotreated CFP-oil properties.

Sample TOS, h	Yield, wt.% dry	Carbon yield, %	H:C, mol:mol	O Content, wt.% dry	Density, g ml^{-1}
45-58	74	87	1.68	0.37	0.850
58-69	79	91	1.74	0.43	0.852
Average	76	89	1.71	0.40	0.851

Hydrotreating successfully removed oxygen and converted the hydroxyaromatics, methoxyphenols, and cycloketones to the corresponding deoxygenated cyclic compounds. The compounds identified by GC-MS in the hydrotreated oils are summarized in Fig. 4, and the major compounds are listed in Table S3. Most of the identified products were cyclic hydrocarbons, consisting of aromatic hydrocarbons, (e.g., benzene derivatives and naphthalenes), and fully or partially hydrogenated hydrocarbons (e.g., cyclohexanes and cyclopentanes, tetralins and decalins). Phenols were the only oxygenated compounds identified and were present in low total concentrations (ca. 1 wt%), consistent with the low product oxygen content. The ^{13}C NMR analysis (Table S4) confirmed that all other oxygenate groups except those associated with phenols were eliminated during hydrotreating. The aliphatic carbon content increased from 30% to over 70%, indicating that hydrotreating resulted in substantial hydrogenation of the aromatic compounds present in the CFP-oil, which is consistent with the GC-MS analysis and the H:C molar ratios (Table 3).

2.4 Fuel Properties of Hydrotreated Products

Fractionation of the hydrotreated oils produced 45 wt% yield of material boiling in the gasoline range (<182 °C atmospheric equivalent temperature, AET) and 39 wt% boiling in the diesel range (182-338 °C AET), with 16 wt% remaining in the residue. These values are in good agreement with those calculated from the SIMDIST analysis (46% for gasoline and 39% for diesel, shown in Fig. S6) and indicate that the majority of the hydrotreated oil (84 wt%) boils in the fuel range.

The detailed hydrocarbon analysis (DHA) analysis (Table S6) indicated that more than 65 wt% of the gasoline-range products consisted of naphthenes (e.g., cyclohexanes and cyclopentanes). Aromatic hydrocarbons were also detected and accounted for 17 wt% of the gasoline fraction. Oxygenated compounds including phenol, methylphenyls, and 2-methoxyphenol were minor products, and the O content of the gasoline fraction was 0.15 wt%. The gasoline fraction exhibited a motor octane number (MON) of 67 and a research octane number (RON) of 62. The diesel fraction had a derived cetane number of 24. Fuel properties have been previously reported for the gasoline fraction from hydrotreated non-catalytic fast pyrolysis oil.[65] Compared to these reported values, the hydrotreated Pt/TiO_2-derived CFP-oils contained considerably more naphthenic compounds with less paraffins and isoparaffins in the gasoline fraction. For products boiling below 150 °C, the octane values from the non-catalytic and CFP processes were similar. However, for products boiling from 150-184 °C, the non-catalytic oils exhibited octane numbers of 38 and 41 for MON and RON, respectively. These values are significantly lower than the octane numbers of 67 (MON) and 62 (RON) reported here. This result suggests an improvement in the overall quality of the gasoline-range product via the CFP process. Despite the improvement over non-catalytic oils, the octane and cetane values reported here are below the minimum fuel requirements (85 for (RON+MON)/2 and 40 for cetane number in the US), and thus, the products are not suitable for direct use as finished fuels. It is possible that the octane value could be improved by controlling the extent of hydrogenation during the hydrotreating step to reduce the concentration of cyclic paraffins. Likewise, the cetane values could be increased by promoting ring opening reactions during CFP or hydrotreating to convert multi-ring compounds into longer chain alkanes. However, even without additional reaction steps, the products could be utilized as blendstocks or co-processed using existing refinery infrastructure. Biorefinery capacities are expected to be an order of magnitude smaller than those of petroleum refineries, and the products could be blended in quantities of <10% with fossil-derived fuels. To the best of our knowledge, these are the first fuel property results reported in the open literature for final, fractionated products generated via a CFP process. While the products were not suitable as finished fuels, the results give valuable guidance for the future development of CFP.

2.5 Technoeconomic and Life-cycle Analysis

Technoeconomic analysis informed by our experimental results indicates a modelled MFSP of \$4.34 GGE^{-1} for CFP using Pt/TiO_2 in a fixed-bed *ex situ* vapor upgrading reactor, with subsequent hydrotreating to reduce the product oxygen content below 1 wt%. This value represents a 16% reduction (\$0.85 GGE^{-1} absolute) compared to a modelled MFSP of \$5.19 GGE^{-1} using HZSM-5 in a circulating-bed reactor.[24, 26] The fixed-bed system offered the advantage of lower catalyst expenses, even when using precious metals, by avoiding constant catalyst replacement necessary due to attrition losses in a circulating-bed system.[27] Sufficient hydrogen was produced from process off-gases and supplemental natural gas was not required for this case. Developing successful and efficient regeneration procedure, confirming long-term catalyst durability, and achieving online times that allow reasonable switching rates between reaction and regeneration systems will be key for commercial implementation of this technology.

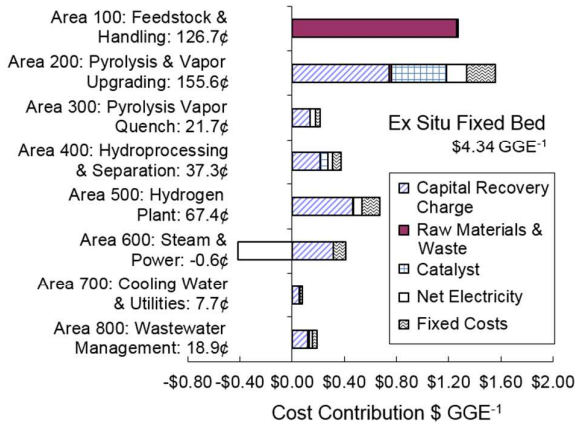

Fig. 6 Modelled cost breakdown (in 2014$) for the production of hydrocarbon fuels via fixed-bed CFP with Pt/TiO_2.

Importantly, fixed-bed CFP is a relatively unexplored research area, and there are many opportunities for technical and economic improvements. In addition to previous sensitivity analyses[27, 66] that show the impacts of various process parameters and underscore the predominant effect of overall carbon efficiency on the economics, our current analysis highlights opportunities for significant cost reductions through catalyst development and optimization of reaction-regeneration conditions. For example, increasing the ratio of online vs. regeneration times has a significant impact on the MFSP by reducing the number of reactors required for the process, decreasing catalyst volume requirements, and lowering the initial capital costs. Calculations in Fig. 7 indicate that increasing the ratio of online vs regeneration time from 0.4 to 2.0 for 2 wt% Pt/TiO_2 would result in a 10% decrease in the MFSP from \$4.34 GGE^{-1} to \$3.89 GGE^{-1}. To this end, mitigating catalyst deactivation during a reaction cycle and/or improving efficiency during regeneration represent economically impactful research targets. These advancements would also reduce the MFSP for lower-cost 0.5 wt% Pt/TiO_2 and Mo_2C catalysts, which are discussed in more detail in Sec. 2.6.

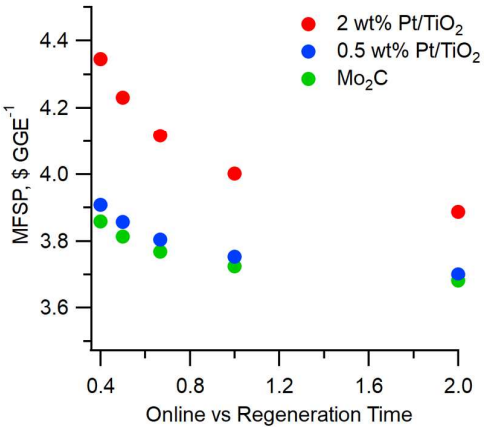

Fig. 7 MFSP of CFP-oil produced over Pt/TiO_2 and Mo_2C catalysts as a function of the ratio of online vs regeneration time.

An associated life-cycle analysis (LCA) focusing on the assessment of the farm-to-wheel (FTW) life cycle carbon intensity highlights the environmental benefits of this process. It exceeds the Renewable Fuel Standard (RFS) greenhouse gas (GHG) emission target for advanced biofuels of at least a 50% reduction from petroleum gasoline.[67] Argonne National Laboratory's Greenhouse gases, Regulated Emissions, and Energy use in Transportation (GREET) model[68] was used to calculate the life cycle GHG emissions. The LCA includes all the stages of a product's life, starting from biomass production and downstream steps involving the extraction of raw materials, the materials' processing, manufacturing, fuel distribution, use, and solid waste disposal. The results quantify emissions for the steps as: feedstock production and logistics (22.6 g CO_{2e}/MJ), fuel production at the biorefinery (0.63 g CO_{2e}/MJ), electricity co-product credit (-6.8 g CO_{2e}/MJ), and fuel transportation and net fuel combustion (1.25 g CO_{2e}/MJ). The resulting total supply chain or life-cycle GHG emissions for the hydrocarbon blendstock produced via the CFP thermochemical conversion pathway was determined to be 17.72 g CO_{2e}/MJ for the \$4.34/GGE modelled MFSP case. This carbon intensity corresponds to an 81.4% GHG reduction compared to conventional gasoline produced from petroleum crudes at 95.29 g CO_{2e}/MJ.

2.6 CFP with Lower-Cost Catalysts

As shown in Fig. 6, catalyst expense is a key contributor to the cost of the pyrolysis and vapor upgrading step (42¢/GGE, Area 200). These calculations informed follow-up experiments which were performed with two lower-cost bifunctional catalysts. These materials include 0.5 wt% Pt/TiO_2 (Class I) and Mo_2C (Class II). The Mo_2C catalyst was prepared using a temperature-programmed reaction method described previously, and the XRD pattern provided in Fig. S7 confirms the orthorhombic phase of the β-Mo_2C catalyst. The Mo_2C catalyst was also characterized for metallic and acidic site densities, and the values provided in Table 4 are consistent with previous reports from our laboratory.[40] The 0.5 wt% Pt/TiO_2 catalyst was prepared using a strong electrostatic adsorption technique to target high Pt dispersion.[69, 70] Characterization data summarized in Table 4 indicate an increased Pt dispersion of 73% compared to the 33% dispersion measured for the 2 wt% Pt/TiO_2 catalyst prepared using incipient wetness methods. Due to the differences in dispersion, the metal site density was similar for 0.5 wt% Pt/TiO_2 and 2 wt% Pt/TiO_2. These data highlight the potential impacts of using targeted synthesis methods to improve the efficiency with which expensive noble metals are utilized. The acidity of the 0.5 wt% Pt/TiO_2 was also similar to that of the 2 wt% Pt/TiO_2 catalyst, as evidenced by the good agreement in acid site density and location of the maximum NH_3-TPD desorption temperature (ca. 350 °C, Fig. S2 and S8). The acid:metal site ratio for the Mo_2C catalyst (12) was higher than the Pt/TiO_2 catalysts, but fell within the range highlighted previously for active HDO catalysts.

Table 4. Summary of characterization results for 2 wt% Pt/TiO_2, 0.5 wt% Pt/TiO_2, and Mo_2C.

Catalyst	Pt dispersion (%)	Metal site density ($\mu mol\ g^{-1}$)	Acid site density ($\mu mol\ g^{-1}$)	Acid: metal site ratio
2 wt% Pt/TiO_2	33	40	220	5.5
0.5 wt% Pt/TiO_2	73	38	190	4.9
$Mo_2C^{\dagger}$	-	54	650	12

†Metal site density is based on H_2 chemisorption experiments.

The materials-only catalyst costs were estimated to be \$204 kg^{-1} for 0.5 wt% Pt/TiO_2 (including 70% salvage value) and \$62 kg^{-1} for Mo_2C (negligible salvage value) using procedures described in the SI. Both of these values represent significant reductions compared to the materials-only cost for the 2 wt% Pt/TiO_2 catalyst, which was estimated at \$805 kg^{-1} with a 75% salvage value at the end of a 2 year lifetime.[71] In order to evaluate the potential economic impact on the process, theoretical MFSP values were calculated in which all TEA parameters were held constant to the values reported in Sec. 2.5, with the exception of catalyst cost. These data indicate that the modelled MFSP of \$4.34 GGE could be reduced to \$3.91 and \$3.86 GGE^{-1} by using 0.5 wt% Pt/TiO_2 and Mo_2C, respectively. Reaching these MFSP values requires the lower-cost catalysts to achieve similar performance to the 2 wt% Pt/TiO_2 material. As a preliminary assessment of this possibility, CFP experiments were performed with 0.5 wt% Pt/TiO_2 and Mo_2C under identical reaction conditions as the 2 wt% Pt/TiO_2 catalyst. As shown in Table 5, the carbon yield and oxygen content of the Mo_2C-derived-CFP-oil was 37% and 18 wt% respectively, and after an initial break-in period, the 0.5 wt% Pt/TiO_2 catalyst stabilized to produce an oil with 42% carbon yield and 19 wt% oxygen. A full description of the CFP-oil composition and gas yields for 0.5 wt% Pt/TiO_2 and Mo_2C catalysts are provided in Table S7-S8. It is important to emphasize that these experiments focused exclusively on a single CFP reaction cycle, and the development of effective regeneration procedures for Mo_2C represents an important research target moving forward. Also, follow-up hydrotreating and fuel testing experiments are necessary to confirm that the CFP-oil derived from the lower-cost catalysts does not have major effects on down-stream processing steps. Nonetheless, the data presented here offer early proof-of-concept that the lower-cost catalysts can be effective for CFP and provide a route towards significant reductions in the MFSP.

Table 5. A comparison of CFP data from 2 wt% Pt/TiO_2 and lower-cost catalysts.

Catalyst	Oil C yield, %	Oxygen Content, wt% dry
2 wt% Pt/TiO_2	38	16
0.5 wt% Pt/TiO_2	42	19
Mo_2C	37	18

3. Conclusions

In this report, we demonstrate that CFP performance (e.g., carbon yield and oil oxygen content) can be improved by using bifunctional metal-acid catalysts in a fixed-bed reactor with co-fed H_2 at near atmospheric pressure, as compared to currently available performance results from a ZSM-5 catalyst operated in a circulating-bed reactor. Fuel property analysis of the hydrotreated fixed-bed CFP-oils showed high selectivity to gasoline- and distillate-range hydrocarbons, and TEA indicated a modelled MFSP of \$4.34 GGE^{-1}, which represents a reduction of \$0.85 compared to values reported for a zeolite-based CFP process. Collectively, these data highlight the potential of CFP as an important part of an integrated biomass-to-fuels pathway. Additional performance enhancements and cost reductions can be achieved through optimization of the catalysts and process conditions. To this end, more research is necessary to improve catalyst stability, understand the effect of acid:metal site ratio on CFP performance, develop efficient regeneration procedures, and validate catalyst lifetimes. Future research should also focus on improving fuel quality, potentially by controlling the extent of hydrogenation and promoting ring-opening reactions to boost octane and cetane values.

4. Experimental

4.1 Materials

Experiments were conducted using southern yellow pine (42 wt% cellulose, 21 wt% hemicellulose, and 30 wt% lignin) supplied by Idaho National Laboratory. The elemental analysis on dry biomass showed that it contains 50 wt% carbon, 43 wt% oxygen, 6 wt% hydrogen, and less than 0.1 wt% nitrogen. The TiO_2 support was obtained from Evonik Resource Efficiency GmbH (Aerolyst® 7711) and was used as received. Tetraammineplatinum nitrate ($Pt(NH_3)_4(NO_3)_2$) was obtained from Strem Chemicals and used as received. Ammonium paramolybdate ($(NH_4)_6Mo_7O_{24}{\cdot}4H_2O$) was obtained from Alfa-Aesar and used as received.

4.2 Catalyst Preparation

The 2 wt% Pt/TiO_2 catalyst was prepared by a standard incipient wetness impregnation. The incipient wetness point of the TiO_2 support was determined to be 0.52 mL g^{-1} by soaking the TiO_2 pellets in excess deionized water for at least 8 h. An aqueous solution containing 11.02 g of $Pt(NH_3)_4(NO_3)_2$ was

added dropwise to 105.2 g of TiO_2 which corresponds to a theoretical Pt loading of 5.3 wt%. In order to ensure complete dissolution of $Pt(NH_3)_4(NO_3)_2$, the aqueous solution was sonicated and heated using a water bath held at 40 °C. The impregnated materials were allowed to soak under a Parafilm vapor barrier overnight, and were subsequently dried at room temperature for > 48 h. The catalyst was reduced *ex situ* at 450 °C in flowing 5% H_2/N_2 for 2 h (5 °C min^{-1} heating rate) and passivated at room temperature in flowing 1% O_2/N_2 prior to reaction testing.

In a separate preparation, 100 g of Pt/TiO_2 with highly dispersed Pt particles was synthesized via strong electrostatic adsorption[69, 70] at a pH of 11.5 using 1.98 g of $Pt(NH_3)_4(NO_3)_2$ to target a Pt loading of 1.0 wt%. The catalyst was soaked for > 24 h in an aqueous solution with a surface loading of 500 $m^2 L^{-1}$ (5.7×10^{-4} M Pt). After impregnation, the catalyst was dried at room temperature for >24 h and then at 60 °C overnight. The dried catalyst was reduced in flowing 5% H_2/N_2 at 450 °C and passivated in flowing 1% O_2/N_2 at room temperature before being loaded into the reactor.

The Mo_2C catalyst was prepared by adapting a temperature-programmed reaction method described previously.[40-42] Briefly, 25 g of ammonium paramolybdate (AM) was sieved to 355-500μm and loaded into a quartz tube reactor on top of a quartz wool plug. The AM was reduced and carburized in 15% CH_4/H_2 flowing at 2500 mL min^{-1}. The sample temperature was increased from room temperature to 200 °C at 10 °C min^{-1}, followed by heating from 200 to 590 °C at 1 °C min^{-1}. The sample remained at 590 °C for 4 h before passively cooling to room temperature in 15% CH_4/H_2. The resulting material was passivated with 1% O_2/He for >12 h and then stored in an Ar-filled glovebox until use. This procedure was repeated five times, and the product was combined to generate sufficient quantity of Mo_2C for reaction testing. Prior to biomass vapor upgrading experiments, the Mo_2C catalyst was pre-reduced *in situ* in flowing H_2 at 400 °C.

4.3 Catalyst Characterization

Powder XRD data were collected using a Rigaku Ultima IV diffractometer with a Cu Kα source (40 kV, 44 mA). Diffraction patterns were collected in the 2θ range of 20–80 degrees at a scan rate of 4 ° min^{-1}. Samples (10–20 mg) were supported on a glass sample holder with a 0.2 mm recessed sample area and were pressed into the recession with a glass slide to obtain a uniform z-axis height. Data were compared to reference card files from the International Center for Diffraction Data (Pt: 00-004-0802, Rutile TiO_2: 00-001-1292, Anatase TiO_2: 00-001-0562, Mo_2C: 01-071-6028) to confirm the identity and phase of the sample. Samples for transmission electron microscopy (TEM) were dropcast onto carbon-coated copper grids (Ted Pella part no. 01824) from chloroform or hexanes suspensions. Imaging was performed using a FEI G20 Tecnai operating at 200 keV. Elemental analysis was performed by Galbraith Laboratories (Knoxville, TN) using inductively coupled plasma optical emission spectroscopy (ICP-OES).

Ammonia temperature programmed desorption (NH_3-TPD) was performed on an Altamira Instruments AMI-390 system equipped with a thermal conductivity detector (TCD) and assuming a NH_3:acid site stoichiometry of 1:1. Catalyst samples (50 mg for Mo_2C, 100-200 mg for Pt/TiO_2 samples) were loaded into a quartz U-tube reactor and held as a fixed bed on a plug of quartz wool. Samples were reduced in flowing 5% H_2/Ar by heating at 5 °C min^{-1} to 450 °C (400 °C for Mo_2C) and then holding at this temperature for 2 h. The samples were cooled to 120 °C in flowing He for 1 h, dosed with flowing 10% NH_3/He for 1 h, and physisorbed NH_3 was purged for 1 h with flowing He. TPD of NH_3 was performed by heating the sample from 120 to 450 °C (400 °C for Mo_2C) at 30 °C min^{-1}. The temperature was then held at 450 °C (400 °C for Mo_2C) for 30 min to allow any remaining NH_3 to desorb without increasing the temperature above the activation temperature. Desorbed NH_3 was measured with the TCD, and calibration was performed after each experiment by introducing five pulses of 10% NH_3/He through a 5 mL sample loop into a stream of flowing He.

The density of metal sites on Mo_2C was measured from chemisorbed H_2 isotherms collected at 40 °C (P = 10.7-74.7 kPa) using a Quantachrome Autosorb 1-C. The samples were reduced under flowing H_2 at 400 °C for 2 h, then evacuated at 400 °C for 2 h. The H*-site (metal site) density was calculated from the difference of the combined and weak isotherms to determine the monolayer coverage of H*-sites per gram of catalysts assuming a H*:M stoichiometry of 1:1.

CO pulse chemisorption was performed using an Altamira Instruments AMI-390 system equipped with a TCD. Catalyst samples (50-100 mg) were loaded into a quartz U-tube reactor and held as a fixed bed on a plug of quartz wool. Samples were reduced in flowing 5% H_2/Ar by heating at 5 °C min^{-1} to 450 °C and then holding at this temperature for 2 h. After the reduction step, catalyst samples were flushed with He (50 mL min^{-1}) for 1 h to remove any weakly adsorbed hydrogen. The samples were then cooled to 30 °C and dosed with sequential 500 μL pulses of a 10% CO/He gas mixture. A 500 μL sample loop was used to calibrate the TCD response for CO after each experiment.

4.4 CFP Reaction Testing

Ex situ CFP experiments were performed in a fluidized-bed pyrolyzer system equipped with a down-stream fixed-bed upgrading reactor. The pyrolysis system and the oil condensation system have been described elsewhere.[22, 55] Southern pine was pyrolyzed in a 5.2-cm inner diameter bubbling fluidized-bed reactor, char was separated in a cyclone and fines in a hot gas filter, and the pyrolysis vapors and gases were passed through a fixed-bed reactor containing the catalyst. The upgraded vapors from the reactor were condensed in an air-cooled condenser followed by an electrostatic precipitator (ESP), a dry-ice trap followed by an iced coalescing filter and a second dry-ice trap. The composition of the upgraded vapors was monitored during the experiments by a residual gas analyzer (RGA) and the exit

gases were analyzed by an Agilent 490 micro GC for CO_2, CO, C_1-C_4 hydrocarbons, and H_2. The product gas flow was measured by a dry gas meter. Gas bag samples were taken intermittently from the exit gases and analyzed by a GC-MS/FID (Agilent 7890B-connected to 5977A MSD and FID).

Several catalytic cycles with intermediate catalyst regeneration and reduction were completed. The pyrolysis and upgrading reactor temperatures were 500 °C and 400 °C, respectively. A catalytic upgrading temperature of 400 °C represents a practical minimum which avoids condensation of the pyrolysis vapors. Higher temperatures are undesirable due to a decrease in hydrogen coverage and thermodynamic limitations on ring hydrogenation, which inhibit HDO reaction pathways. The catalyst mass in the upgrading reactor was approximately 100 g and biomass was fed at a rate of 150 g h^{-1} to achieve a WHSV of 1.5 h^{-1}. Based on a measured char yield of 10 wt% in the pyrolysis reactor (Table 2), the corresponding WHSV based on vapor products to the fixed bed is estimated to be 1.35 h^{-1}. All experiments were performed at atmospheric pressure. A gas mixture containing 85% H_2/15% N_2 was introduced at a rate 17.6 sL min^{-1} during the catalytic cycle to achieve a hydrogen partial pressure of 0.08 MPa. Before each catalytic cycle, the catalyst was reduced in the same H_2/N_2 gas flow for 2 h at 450 °C. Regeneration of the catalyst was performed at 450 °C in a flow of 0.2 sL min^{-1} air and 10 sL min^{-1} nitrogen overnight. The partial pressure of air was minimized during catalyst regeneration to prevent the formation of hot spots in the catalyst bed. However, subsequent experiments confirmed that the catalyst could be effectively regenerated in 2.5 h by incrementally increasing the partial pressure of air.

The product liquids from the condenser, ESP, and the dry-ice traps were combined and allowed to phase separate into organic and aqueous phases. The liquid-phase yields (oil and aqueous) were determined by the mass gain in the condensation system and the ratios of the separated liquids. The gas yields were calculated from the microGC and exit gas flow measurements. The carbonaceous products in the gas bag samples were quantified, and any condensable products (oxygenates and $C5_{5+}$ hydrocarbons) were added to the total oil yield because these compounds are expected to be condensed more efficiently in a larger scale reactor with less dilute vapors. Char was determined from the mass gain in the pyrolyzer, cyclone, and hot gas filter, and coke from the CO_2 and CO signals during catalyst regeneration. The liquids were analyzed for carbon, hydrogen, and nitrogen (ASTM D5291/D5373) using a LECO TruSpec® CHN analyzer. Oxygen was determined by difference. Calibration of the CHN analyzer was performed with a known standard (EDTA). The CFP-oil water content was determined by Karl Fischer titration. GC–MS analysis of the samples was performed using an Agilent G1530A GC equipped with an Agilent 5973 mass-selective detector. 1 µl samples of oil diluted 1:10 in acetone were injected into the GC, which contained a 30 m x 0.25 mm x 0.25 µm Restek Rtx-50 (50%-phenyl-methylpolysiloxane phase) column. The GC oven temperature was held at 40 °C for 2 min, ramped to 140 °C at 7 °C min^{-1}, then to 290 °C at 12 °C min^{-1} and held for 5 min. The inlet temperature was 250 °C, transfer line temperature 300 °C, and there was a helium carrier gas flow of 1 ml min^{-1} with a split ratio of 10:1. Semi-quantitative analysis was performed based on 18 calibration compounds typical of those observed in CFP-oils (Table S9).

Carbon-13 nuclear magnetic resonance (NMR) spectra were taken in a 500-MHz Varian Unity Plus spectrometer with samples in deuterated dimethyl sulfoxide (d6-DMSO) and a relaxation agent, chromium(II) acetylacetonate. Spectra were processed by using Mestre-Nova software, and the results were classified by previously described methods.[72]

4.5 Hydrotreating

A commercial Ni-Mo sulfide hydrotreating catalyst and a bench-scale hydrotreater were used for the CFP-oil hydrotreating test. The hydrotreater was configured as a single-pass, concurrent, continuous, down-flow reactor. It is described in detail in a previous publication.[60] The reactor was Hastelloy C tubing with a 1.3 cm internal diameter and 63.5 cm in length. Mass flow controllers were used to feed H_2 and ISCO pumps were used to feed bio-oil and sulfiding liquid. After exiting the catalytic reactor, the liquid products were separated from the gaseous products in pressurized and cooled traps. The recovered liquid products were collected, phase-separated, weighed, and sampled for further analysis. The off-gas passed through the back-pressure regulator and was then directed through a DryCal gas meter to measure the gas flow rate and analyzed by an online Inficon Micro-GC 3000 four-channel micro-GC. 20 ml (9.4 g) catalyst was used for the run and prior to the experiment, the catalyst was pre-sulfided by heating to 150 °C in H_2 flow, keeping at 150 °C for 2 h in flow of H_2 and sulfiding liquid (35% di-tert-butyl disulfide (DTBDS) in decane), heating from 150 to 400 °C in 3 h and the holding 400 °C for 4 h with H_2 and sulfiding agent flowing. The operating pressure was 13.0 MPa, and the sulfiding agent liquid hourly space velocity (LHSV) was 0.12 L L^{-1} of catalyst h^{-1}.

DTBDS was added to the CFP-oil feed to maintain 150 ppm S. A 82 h test at bio-oil LHSV of 0.20 h^{-1} was completed after which an additional 58 h test at LHSV of 0.30 h^{-1} was conducted. The liquid products and outlet gas analysis data were collected over the entire period with individual products and data sets collected in operating windows of 12 h. The hydrogen consumption in g H_2 per g dry feed was calculated based on the bio-oil flow rate and the difference of hydrogen inlet and outlet flowrate. The hydrogen outlet flowrate was calculated by the total outlet flow rate, based on the measured outlet flowrate by the volumetric gas flow meter with deduction of flowrate increase caused by accumulation of liquid in the reactor system, and the hydrogen concentration measured by the micro-GC. The yields of oil and gas products were determined based on the weight of oil product and the outlet gas flow rate and composition.

The methods described for CFP-oil analysis were also applied for the hydrotreated products. Density measurements were conducted on a Stabinger viscometer (Anton Paar SVM

3000) at 25 °C. Simulated distillation was conducted by using SimDis ASTM D2887 to estimate distribution of fuels blend based on boiling point.

4.6 Oil Fractionation and Fuel Property Analysis

Gasoline and diesel fractions were separated from the hydrotreated oils by distillation in a B/R 800 micro spinning band distillation system. Lights boiling below 160 °C were separated by atmospheric distillation and higher boiling components by vacuum distillation at 0.7 kPa (5 torr). The fractions boiling below atmospheric equivalent temperature (AET) of 182 °C were characterized by DHA according to ASTM D6729. The samples were analyzed twice, once with GC/FID for quantitative analysis according to the method, and again using the same GC parameters but with the mass spectrometer to confirm compound identification. The fraction with AET of 182-320 °C was analyzed for derived cetane number (DCN) according to ASTM method D6890.

4.7 Technoeconomic and Life-cycle Analysis

Data from the experiments were used in a conceptual process model in Aspen Plus™ reflecting a potential scaled-up implementation of this technology. This process model provided insights into current catalytic reactor performance with respect to bottlenecks and potential improvements to reduce costs. The process design was similar to that proposed earlier.[27] The key difference of this design compared to the previous study is the use of only one *ex situ* fixed-bed reactor system (vs. two systems in series) to reflect the current experiments. Fig. 10 shows a simplified block flow diagram of the process used for the TEA model; a brief description is included here, with further design details available in previous publications.[27, 66] 2000 dry metric tons day^{-1} of low-ash woody feedstock is fast pyrolyzed, with heat provided to the circulating-bed material by combusting the char from fast pyrolysis. The produced vapors are separated from the solids via cyclones, and further filtered to remove fines, before being processed in a fixed-bed *ex situ* vapor upgrading system. Hot gas filtration is required to prevent catalyst fouling and poisoning in the fixed-bed reactor. The fixed-bed system has spare reactors to regenerate coked catalyst; the number of online and spare reactors in the process design is dictated by on-stream and regeneration times. The upgraded vapors from the fixed-bed reactors are condensed, with the separation of two liquid phases (organic and aqueous), and off gases are partly used for fast pyrolysis reactor fluidization, with the remainder used for hydrogen production or as a fuel gas in the process. The fast pyrolysis reactor fluidization gas is enriched with hydrogen; note that the hydrogen partial pressure in the feed gas (0.61 MPa) is higher than in our experimental system (~0.085 MPa). The moderate total pressure (0.85 MPa) in the design [27, 66] was adopted to allow lower capital costs by reducing equipment sizes.

The aqueous phase from the condensation system is sent to a wastewater management system; in the current design the organic carbon is combusted in a regenerative thermal oxidizer; other designs, not discussed here, can include recovery of the organic species for co-products.[73-75]

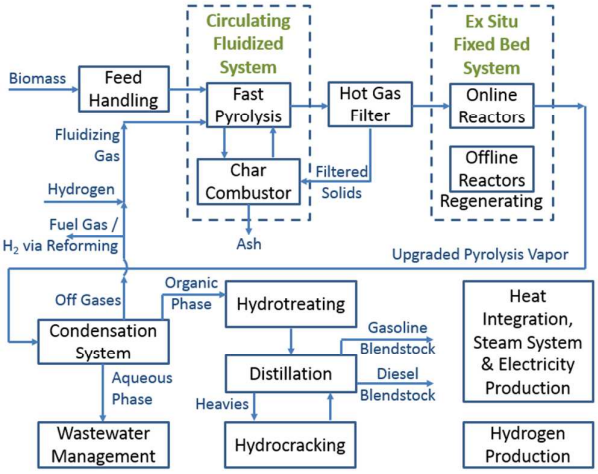

Fig. 10. A simplified block flow diagram outlining the conceptual process utilized for the TEA model.

The organic phase is sent to a hydroprocessing and product recovery system, involving a hydrotreater for hydrodeoxygenation (to reduce the product oxygen content below 1wt%), distillation for the recovery of gasoline- and diesel-range blendstock streams, and a hydrocracker to process heavier species into the gasoline and diesel ranges. The experimental hydrotreating carbon efficiency (normalized) was 93%. Distillation results showed that 16 wt% of the fuel blendstock was heavier than the diesel-boiling range, hence there is a need for hydrocracking unit to crack the heavier material to the gasoline and diesel ranges. The modeled overall hydroprocessing carbon efficiency was reduced to 91%, assuming an additional 2% loss in carbon efficiency during hydrocracking; this assumption is similar to examples from petroleum refining projections of C_3 and lighter material from hydrocracking;[76] this metric is expected to be experimentally verified for our products in the future.

The process design and costs include units for heat recovery, steam generation, electricity production, cooling water and other utilities. Hydrogen is produced in a steam reformer from process off-gases, and pressure swing adsorption units are used for hydrogen recovery from hydrogen-rich streams; in this design sufficient off-gases are available to meet all the hydrogen demand. Excess off-gases are combusted to produce steam and electricity; excess electricity is sold to the grid.

Key assumptions for the analysis include: feedstock with elemental analysis of C:50.94 wt%, H:6.04 wt%, N:0.17 wt%, S:0.03 wt%, O:41.90 wt%, Ash:0.92 wt% on a dry basis, and 10 wt% moisture, at a cost of $79 dry metric ton^{-1},[77] mature plant design and operations, without the uncertainties associated with pioneer plants allowing 90% on-stream time; 60% debt financing at 8% annual interest rate for 10 years; 10% return on the remaining 40% equity financing; a plant life of 30 years; plant depreciation over 7 years, with the steam plant

depreciating over 20 years; 35% income tax rate; a three year construction period with 6 months for startup. A discounted cash flow rate of return analysis is used to calculate a Minimum Fuel Selling Price (MFSP) in 2014 dollars. Process assumptions for the *ex situ* fixed-bed upgrading and hydrotreating operations were consistent with those shown in Tables 2 and 3; yields were normalized to close the mass and atomic balances before using the experimental results in the process model. The methods for calculating life-cycle GHG emissions using GREET have been previously documented.[78]

Conflicts of Interest

There are no conflicts to declare.

Acknowledgements

This research was supported by the U.S. Department of Energy (DOE), Office of Energy Efficiency and Renewable Energy (EERE), Bioenergy Technologies Office (BETO), under Contract DE-AC36-08-GO28308 at the National Renewable Energy Laboratory (NREL), Contract DE-AC06-76RLO-1830 at the Pacific Northwest National Laboratory (PNNL), Contract DE-AC02-06CH11357 at the Argonne National Laboratory (ANL), and in collaboration with the Chemical Catalysis for Bioenergy Consortium (ChemCatBio), a member of the Energy Materials Network (EMN). The authors would like to thank Scott Palmer, Lisa Fouts, Anne Starace, Susan Habas, Kylie Smith, and Renee Happs at NREL as well as Igor Kutnyakov, Benjamin Roberts, Richard Lucke, and Suh-Jane Lee at PNNL for assistance with catalyst characterization, reactor operation, and product analysis.

Disclaimer

The views expressed in the article do not necessarily represent the views of the U.S. Department of Energy or the United States Government.

References

1. R. A. Efroymson, M. H. Langholtz, K. E. Johnson and B. J. Stokes, *2016 Billion-Ton Report: Advancing Domestic Resources for a Thriving Bioeconomy, Volume 2: Environmental Sustainability Effects of Select Scenerios from Volume 1*, U. S. Department of Energy Oak Ridge National Laboratory, 2016.
2. M. H. Langholtz, B. J. Stokes and L. M. Eaton, *2016 Billion-Ton Report: Advancing Domestic Resoruces for a Thriving Bioeconomy, Volume I: Economic Avaiability of Feedstocks*, U.S. Department of Energy Oak Ridge National Laboratory, 2016.
3. J. C. Serrano-Ruiz and J. A. Dumesic, *Energy & Environmental Science*, 2011, **4**, 83-99.
4. D. A. Ruddy, J. A. Schaidle, J. R. Ferrell Iii, J. Wang, L. Moens and J. E. Hensley, *Green Chem.*, 2014, **16**, 454-490.
5. A. V. Bridgwater, *Fast Pyrolysis of Biomass: A Handbook*, CPL Press, Newbury, UK, 1999.
6. A. V. Bridgwater, *Fast Pyrolysis of Biomass: A Handbook Volume 2*, CPL Press, Newbury, UK, 2002.
7. A. V. Bridgwater, *Fast Pyrolysis of Biomass: A Handbook Volume 3*, CPL Press, Newbury, UK, 2005.
8. A. d. R. Pinho, M. B. B. de Almeida, F. L. Mendes, L. C. Casavechia, M. S. Talmadge, C. M. Kinchin and H. L. Chum, *Fuel*, 2017, **188**, 462-473.
9. A. d. R. Pinho, M. B. B. de Almeida, F. L. Mendes, V. L. Ximenes and L. C. Casavechia, *Fuel Process. Technol.*, 2015, **131**, 159-166.
10. S. Czernik and A. V. Bridgwater, *Energy Fuels*, 2004, **18**, 590-598.
11. T. L. Marker, L. G. Felix, M. B. Linck and M. J. Roberts, *Environ. Prog. Sustain.*, 2012, **31**, 191-199.
12. T. L. Marker, L. G. Felix, M. B. Linck, M. J. Roberts, P. Ortiz-Toral and J. Wangerow, *Environ. Prog. Sustain.*, 2014, **33**, 762-768.
13. M. Linck, L. Felix, T. Marker and M. Roberts, *Wiley Interdisciplinary Reviews: Energy and Environment*, 2014, **3**, 575-581.
14. V. K. Venkatakrishnan, W. N. Delgass, F. H. Ribeiro and R. Agrawal, *Green Chem.*, 2015, **17**, 178-183.
15. T. R. Carlson, J. Jae, Y.-C. Lin, G. A. Tompsett and G. W. Huber, *J. Catal.*, 2010, **270**, 110-124.
16. C. Mukarakate, X. Zhang, A. R. Stanton, D. J. Robichaud, P. N. Ciesielski, K. Malhotra, B. S. Donohoe, E. Gjersing, R. J. Evans, D. S. Heroux, R. Richards, K. Iisa and M. R. Nimlos, *Green Chem.*, 2014, **16**, 1444-1461.
17. V. Paasikallio, C. Lindfors, E. Kuoppala, Y. Solantausta, A. Oasmaa, J. Lehto and J. Lehtonen, *Green Chem.*, 2014, **16**, 3549.
18. R. French and S. Czernik, *Fuel Process. Technol.*, 2010, **91**, 25-32.
19. J. D. Adjaye and N. N. Bakhshi, *Fuel Process. Technol.*, 1995, **45**, 161-183.
20. T. R. Carlson, Y.-T. Cheng, J. Jae and G. W. Huber, *Energy & Environmental Science*, 2011, **4**, 145-161.
21. V. Paasikallio, K. Kalogiannis, A. Lappas, J. Lehto and J. Lehtonen, *Energy Technology*, 2017, **5**, 94-103.
22. K. Iisa, R. J. French, K. A. Orton, M. M. Yung, D. K. Johnson, J. ten Dam, M. J. Watson and M. R. Nimlos, *Energy Fuels*, 2016, **30**, 2144-2157.
23. K. Iisa, R. J. French, K. A. Orton, S. Budhi, C. Mukarakate, A. R. Stanton, M. M. Yung and M. R. Nimlos, *Top. Catal.*, 2015, **59**, 94-108.
24. M. S. Talmadge, A. Dutta, J. R. Ferrell and E. Tan, *NREL Thermochemical Platform Analysis*, BETO, Denver, CO, 2017.
25. E. Taarning, C. M. Osmundsen, X. Yang, B. Voss, S. I. Andersen and C. H. Christensen, *Energy & Environmental Science*, 2011, **4**, 793-804.
26. U.S. Department of Energy Bioenergy Technologies Office Multi-Year Program Plan March 2016, https://energy.gov/sites/prod/files/2016/03/f30/mypp_beto_march2016_2.pdf).
27. A. Dutta, J. A. Schaidle, D. Humbird, F. G. Baddour and A. Sahir, *Top. Catal.*, 2016, **59**, 2-18.
28. M. Saidi, F. Samimi, D. Karimipourfard, T. Nimmanwudipong, B. C. Gates and M. R. Rahimpour, *Energy & Environmental Science*, 2014, **7**, 103-129.
29. S. Boonyasuwat, T. Omotoso, D. E. Resasco and S. P. Crossley, *Catal. Lett.*, 2013, **143**, 783-791.

30. T. Omotoso, S. Boonyasuwat and S. P. Crossley, *Green Chem.*, 2014, **16**, 645-652.
31. M. B. Griffin, G. A. Ferguson, D. A. Ruddy, M. J. Biddy, G. T. Beckham and J. A. Schaidle, *ACS Catal.*, 2016, **6**, 2715-2727.
32. T. O. Omotoso, B. Baek, L. C. Grabow and S. P. Crossley, *ChemCatChem*, 2017, **9**, 2642-2651.
33. P. M. de Souza, L. Nie, L. E. P. Borges, F. B. Noronha and D. E. Resasco, *Catal. Lett.*, 2014, **144**, 2005-2011.
34. P. M. de Souza, R. C. Rabelo-Neto, L. E. P. Borges, G. Jacobs, B. H. Davis, T. Sooknoi, D. E. Resasco and F. B. Noronha, *ACS Catal.*, 2015, **5**, 1318-1329.
35. C. A. Teles, R. C. Rabelo-Neto, G. Jacobs, B. H. Davis, D. E. Resasco and F. B. Noronha, *ChemCatChem*, 2017, **9**, 2850-2863.
36. R. C. Nelson, B. Baek, P. Ruiz, B. Goundie, A. Brooks, M. C. Wheeler, B. G. Frederick, L. C. Grabow and R. N. Austin, *ACS Catal.*, 2015, **5**, 6509-6523.
37. W.-S. Lee, A. Kumar, Z. Wang and A. Bhan, *ACS Catal.*, 2015, **5**, 4104-4114.
38. W.-S. Lee, Z. Wang, R. J. Wu and A. Bhan, *J. Catal.*, 2014, **319**, 44-53.
39. C.-J. Chen, W.-S. Lee and A. Bhan, *Appl. Catal., A*, 2016, **510**, 42-48.
40. F. G. Baddour, V. A. Witte, C. P. Nash, M. B. Griffin, D. A. Ruddy and J. A. Schaidle, *ACS Sustain. Chem. Eng.*, 2017, **5**, 11433-11439.
41. F. G. Baddour, C. P. Nash, J. A. Schaidle and D. A. Ruddy, *Angew. Chem. Int. Ed.*, 2016, **55**, 9026-9029.
42. J. A. Schaidle, J. Blackburn, C. A. Farberow, C. Nash, K. X. Steirer, J. Clark, D. J. Robichaud and D. A. Ruddy, *ACS Catal.*, 2016, **6**, 1181-1197.
43. M. M. Sullivan, C. J. Chen and A. Bhan, *Catalysis Science and Technology*, 2016, **6**, 602-616.
44. M. B. Griffin, F. G. Baddour, S. E. Habas, C. P. Nash, D. A. Ruddy and J. A. Schaidle, *Catalysis Science & Technology*, 2017, **7**, 2954-2966.
45. T. Prasomsri, T. Nimmanwudipong and Y. Román-Leshkov, *Energy and Environmental Science*, 2013, **6**, 1732-1738.
46. T. Prasomsri, M. Shetty, K. Murugappan and Y. Román-Leshkov, *Energy and Environmental Science*, 2014, **7**, 2660-2669.
47. M. Shetty, K. Murugappan, T. Prasomsri, W. H. Green and Y. Román-Leshkov, *J. Catal.*, 2015, **331**, 86-97.
48. Q. Lu, Y. Zhang, Z. Tang, W.-z. Li and X.-f. Zhu, *Fuel*, 2010, **89**, 2096-2103.
49. S. Wan, T. Pham, S. Zhang, L. Lobban, D. Resasco and R. Mallinson, *AIChE J.*, 2013, **59**, 2275-2285.
50. M. A. Machado, S. He, T. E. Davies, K. Seshan and V. Teixeira da Silva, *Catal. Today*, 2017.
51. K. Murugappan, C. Mukarakate, S. Budhi, M. Shetty, M. Nimlos and Y. Roman-Leshkov, *Green Chem.*, 2016, DOI: 10.1039/C6GC01189F.
52. K. Wang, D. C. Dayton, J. E. Peters and O. D. Mante, *Green Chem.*, 2017, **19**, 3243-3251.
53. M. Niwa and N. Katada, *Catal. Surv. Asia*, 1997, **1**, 215-226.
54. B. Liu, D. Slocombe, M. AlKinany, H. AlMegren, J. Wang, J. Arden, A. Vai, S. Gonzalez-Cortes, T. Xiao, V. Kuznetsov and P. P. Edwards, *Applied Petrochemical Research*, 2016, **6**, 209-215.
55. K. Iisa, R. J. French, K. A. Orton, A. Dutta and J. A. Schaidle, *Fuel*, 2017, **207**, 413-422.
56. D. Howe, T. Westover, D. Carpenter, D. Santosa, R. Emerson, S. Deutch, A. Starace, I. Kutnyakov and C. Lukins, *Energy Fuels*, 2015, **29**, 3188-3197.
57. X.-L. Li, J. Deng, J. Shi, T. Pan, C.-G. Yu, H.-J. Xu and Y. Fu, *Green Chem.*, 2015, **17**, 1038-1046.
58. J. Guo, G. Xu, Z. Han, Y. Zhang, Y. Fu and Q. Guo, *ACS Sustain. Chem. Eng.*, 2014, **2**, 2259-2266.
59. T. Nimmanwudipong, C. Aydin, J. Lu, R. C. Runnebaum, K. C. Brodwater, N. D. Browning, D. E. Block and B. C. Gates, *Catal. Lett.*, 2012, **142**, 1190-1196.
60. D. C. Elliott, H. Wang, R. French, S. Deutch and K. Iisa, *Energy Fuels*, 2014, **28**, 5909-5917.
61. D. C. Elliott, *Energy Fuels*, 2007, **21**, 1792-1815.
62. F. A. Agblevor, D. C. Elliott, D. M. Santosa, M. V. Olarte, S. D. Burton, M. Swita, S. H. Beis, K. Christian and B. Sargent, *Energy Fuels*, 2016, **30**, 7947−7958.
63. O. D. Mante, D. C. Dayton, J. Gabrielsen, N. L. Ammitzboll, D. Barbee, S. Verdier and K. Wang, *Green Chem.*, 2016, **18**, 6123-6135.
64. D. C. Elliott, T. R. Hart, G. G. Neuenschwander, L. J. Rotness, M. V. Olarte, A. H. Zacher and Y. Solantausta, *Energy Fuels*, 2012, **26**, 3891-3896.
65. M. V. Olarte, A. B. Padmaperuma, J. R. Ferrell, E. D. Christensen, R. T. Hallen, R. B. Lucke, S. D. Burton, T. L. Lemmon, M. S. Swita, G. Fioroni, D. C. Elliott and C. Drennan, *Fuel*, 2017, **202**, 620-630.
66. A. Dutta, A. Sahir, E. Tan, D. Humbird, L. Snowden-Swan, P. Meyer, J. Ross, D. Sexton, R. Yap and J. Lukas, *Process Design and Economics for the Conversion of Lignocellulosic Biomass to Hydrocarbon Fuels: Thermochemical Research Pathways with In Situ and Ex Situ Upgrading of Fast Pyrolysis Vapors*, NREL/TP-5100-62455 and PNNL-23823, 2015.
67. United States Environmental Protection Agency Renewable Fuel Standard Program, https://www.epa.gov/renewable-fuel-standard-program).
68. Argonne National Laboratory: Greenhouse Gases, Regulated Emissions and Energy Use in Transportation (GREET) Model, https://greet.es.anl.gov/).
69. J. T. Miller, M. Schreier, A. J. Kropf and J. R. Regalbuto, *J. Catal.*, 2004, **225**, 203-212.
70. M. Schreier and J. R. Regalbuto, *J. Catal.*, 2004, **225**, 190-202.
71. F. G. Baddour and L. Snowden-Swan, Catalyst Cost Model Development. Presented at U.S. Department of Energy (DOE) Bioenergy Technologies Office (BETO) 2017 Project Peer Review Meeting March 7, 2017, https://energy.gov/sites/prod/files/2017/05/f34/thermochem_baddour_2.5.4.301-302.pdf).
72. R. M. Happs, K. Iisa and J. R. Ferrell Iii, *RSC Adv.*, 2016, **6**, 102665-102670.
73. A. N. Wilson, M. J. Price, C. Mukarakate, R. Katahira, M. B. Griffin, J. R. Dorgan, J. Olstad, K. A. Magrini and M. R. Nimlos, *ACS Sustain. Chem. Eng.*, 2017, **5**, 6615-6625.
74. A. K. Starace, B. A. Black, D. D. Lee, E. C. Palmiotti, K. A. Orton, W. E. Michener, J. ten Dam, M. J. Watson, G. T. Beckham, K. A. Magrini and C. Mukarakate, *ACS Sustain. Chem. Eng.*, 2017, **5**, 11761-11769.
75. L. N. Jayakody, C. W. Johnson, J. M. Whitham, R. J. Giannone, B. A. Black, N. S. Cleveland, D. M. Klingeman,

W. E. Michener, J. L. Olstad, D. R. Vardon, R. C. Brown, S. D. Brown, R. L. Hettich, A. M. Guss and G. T. Beckham, *Energy & Environmental Science*, 2018, DOI: 10.1039/C8EE00460A.

76. J. H. Gary and G. E. Handwerk, *Petroleum Refining Technology and Economics*, Marcel Dekker, New York, NY, 3rd edition edn., 1994.

77. D. Hartley, D. N. Thompson, H. Hu and H. Cai, *Woody Feedstock 2017 State of Technology Report*, Idaho National Laboratory, 2017.

78. F. K. Adom, H. Cai, J. B. Dunn, D. Hartley, E. Searcy, E. Tan, S. Jones and L. Snowden-Swan, *Supply Chain Sustainability Analysis of Fast Pyrolysis and Hydrotreating Bio-Oil to Produce Hydrocarbon Fuels*, Argonne National Lab.(ANL), Argonne, IL (United States), 2016.

Driving towards cost-competitive biofuels through catalytic fast pyrolysis by rethinking catalyst selection and reactor configuration

Michael B. Griffin,[a,‡] Kristiina Iisa,[a,‡] Huamin Wang,[b] Abhijit Dutta,[a] Kellene A. Orton,[a] Richard J. French,[a] Daniel M. Santosa,[b] Nolan Wilson,[a] Earl Christensen,[a] Connor Nash,[a] Frederick Baddour,[a] Kurt Van Allsburg,[a] Daniel A. Ruddy,[a] Eric C. D. Tan,[a] Hao Cai,[c] Calvin Mukarakate,[a] Joshua A. Schaidle[a,*]

[a] *National Renewable Energy Laboratory, 15523 Denver West Pkwy., Golden, CO 80401, USA.*
[b] *Pacific Northwest National Laboratory, 902 Battelle Blvd., Richland, WA 99352 USA*
[c] *Argonne National Laboratory, 9700 Cass Ave., Lemont, IL 60439*
‡These authors contributed equally to the article.
**Corresponding author: Joshua.Schaidle@nrel.gov*

TOC GRAPHIC

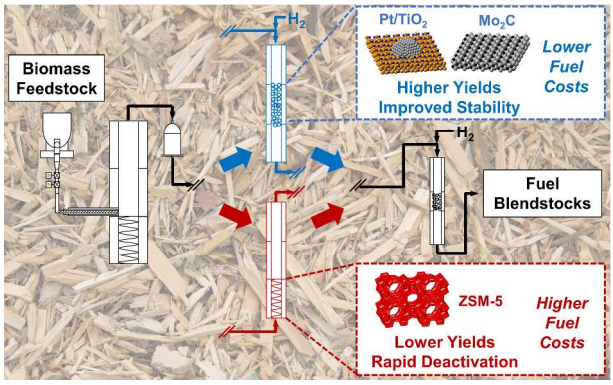

Bifunctional fixed-bed catalysts improve the deoxygenation of biomass pyrolysis vapors and reduce the production cost of renewable hydrocarbon fuels.